Journal of Power Sources 188 (2009) 323–331

Contents lists available at ScienceDirect

Journal of Power Sources

journal homepage: www.elsevier.com/locate/jpowsour

Electrodeposited manganese oxides on three-dimensional carbon nanotube substrate: Supercapacitive behaviour in aqueous and organic electrolytes

Kyung-Wan Nam[a,b], Chang-Wook Lee[a], Xiao-Qing Yang[b], Byung Won Cho[c], Won-Sub Yoon[d,**], Kwang-Bum Kim[a,*]

[a] Division of Materials Science and Engineering, Yonsei University, 134 Shinchon-dong, Seodaemoon-gu, Seoul 120-749, Republic of Korea
[b] Chemistry Department, Brookhaven National Laboratory, Upton, NY 11973, USA
[c] Battery Research Center, Korea Institute of Science and Technology, 39-1 Hawolgok-dong Seongbuk-gu, Seoul 130-650, Republic of Korea
[d] School of Advanced Materials Engineering, Kookmin University, 861-1 Jeongneung-dong, Seongbuk-gu, Seoul 136-702, Republic of Korea

ARTICLE INFO

Article history:
Received 18 July 2008
Received in revised form 4 October 2008
Accepted 11 November 2008
Available online 11 December 2008

Keywords:
Supercapacitor
Nanocomposite
Organic electrolyte
Manganese oxide
Carbon nanotube
Specific energy

ABSTRACT

Thin amorphous manganese oxide layers with a thickness of 3–5 nm are electrodeposited on a carbon nanotube (CNT) film substrate that has a three-dimensional nanoporous structure (denoted as MnO_2/CNT electrode). For the purpose of comparison, manganese oxide films are also electrodeposited on a flat Pt-coated Si wafer substrate (denoted as MnO_2 film electrode). The pseudocapacitive properties of the MnO_2 film and MnO_2/CNT electrodes are examined in both aqueous electrolyte (1.0 M KCl) and non-aqueous organic electrolyte (1.0 M $LiClO_4$ in propylene carbonate). While both types of electrode show pseudocapacitive behaviour in the aqueous electrolyte, only the MnO_2/CNT electrode does so in the organic electrolyte, due to its high oxide/electrolyte interfacial area and improved electron conduction through the CNT substrate. Compared with the MnO_2 film electrode, the MnO_2/CNT electrode shows a much higher specific capacitance and better high-rate capability, regardless of the electrolyte used. Use of the organic electrolyte results in a ~6 times higher specific energy compared with that obtained with the aqueous electrolyte, while maintaining a similar specific power. The construction of a three-dimensional nanoporous network structure consisting of a thin oxide layer on a CNT film substrate at the nm scale and the use of an organic electrolyte are promising approaches to improving the specific energy of supercapacitors.

1. Introduction

Manganese oxides in various forms have been widely studied as electrode materials for electrochemical energy storage systems, such as cathode materials in MnO_2/Zn alkaline cells [1], intercalation hosts for lithium batteries [2–7] and, more recently, electrode materials in supercapacitors [8,9]. Compared with other transition metal oxides for supercapacitors such as $RuO_2 \cdot xH_2O$ [10], NiO_x [11,12], CoO_x [13] and V_2O_5 [14,15], manganese oxides have received considerable attention due to their low cost and environmental friendly characteristics. Various methods have been reported for the preparation of manganese oxide materials to serve as electrodes for supercapacitors, such as the sol–gel technique [9,16], solution-based chemical routes [17], electrochemical deposition [18–20], hydrothermal method [21], electrostatic spray deposition (ESD) [22] and sonochemistry [23]. Recently, considerable effort has also been made to synthesize composite materials composed of manganese oxides and carbonaceous materials such as carbon nanotubes (CNTs) [24–27], carbon nanoform [28], exfoliated graphite [29] and ordered mesoporous carbon [30,31]. Most of these studies have focused on the synthesis methods with the goal of achieving enhanced electrochemical performance, e.g., a high specific capacitance, long-term cycling behaviour, and fast charging/discharging rate.

Energy density is one of the critical properties of supercapacitors that needs to be improved for applications such as hybrid electric vehicles (HEVs) and fuel cell vehicles (FCVs). The energy stored in a supercapacitor can be written as

$$\text{energy density} = \frac{1}{2}CV^2 \quad (1)$$

where C and V are the capacitance and operating voltage of the supercapacitor, respectively. Based on Eq. (1), two strategies can be considered to enhance the energy density of a supercapacitor. One is

* Corresponding author. Tel.: +82 2 2123 2839; fax: +82 2 312 5375.
** Corresponding author. Tel.: +82 2 910 4664; fax: +82 2 910 4320.
E-mail addresses: wsyoon@kookmin.ac.kr (W.-S. Yoon), kbkim@yonsei.ac.kr (K.-B. Kim).

0378-7753/$ – see front matter © 2008 Elsevier B.V. All rights reserved.
doi:10.1016/j.jpowsour.2008.11.133

increasing the specific capacitance of the electrode material and the other is increasing the operating voltage. Since the energy density of a supercapacitor is proportional to the square of the operating voltage, the latter strategy is a more effective way to improve the energy density. Unfortunately, most studies on manganese oxide-based electrodes for supercapacitor applications reported in the literature have focused on the use of neutral aqueous electrolytes such as LiCl, NaCl, KCl and Na_2SO_4, which limited the operating voltage range [8,9,16–23,25–31]. Supercapacitors using manganese oxide-based electrodes and aqueous electrolytes may suffer from a low specific energy (Wh kg^{-1}), because of their restricted potential window of approximately 1 V. On the other hand, the use of organic electrolytes would provide stable potential windows of over 4.0 V *vs.* Li/Li^+. Therefore, the development of manganese oxide-based electrodes using organic electrolytes is quite important in enhancing the energy and power density of the corresponding supercapacitors.

There have been extensive studies regarding the use of manganese dioxide (MnO_2) materials with various structural forms (e.g., β, γ, α, δ and amorphous-MnO_2) as electrode materials for rechargeable Li-ion batteries with organic electrolytes [2–7]. Recently, nanocomposite materials composed of manganese oxides and carbon materials (i.e., acetylene black and Ketjen black) were employed as the cathode materials for rechargeable Li-ion batteries [32–34]. Although the charge–discharge curves of these manganese oxide-based materials showed large discrepancies in terms of their features, the Li insertion/desertion behaviour of most manganese oxide-based materials can be characterized by typical S-shaped charge–discharge curves with various voltage plateaux depending on their structural forms or synthetic routes. In order for manganese oxide materials to exhibit pseudocapacitive behaviour in organic as well as aqueous electrolytes, continuous two-dimensional redox reactions over wide potential ranges with fast reaction kinetics are required [35]. Recently, Okubo et al. [36] reported the existence of a nanosize effect on high-rate Li-ion intercalation in $LiCoO_2$ cathode [36]. They demonstrated that the capacitive behaviour became stronger as the crystallite size decreased on the nanometer scale (i.e., 17–6 nm). High electronic conductivity of the manganese oxide electrode is also crucial for its application to pseudocapacitors. Thus, the preparation of a very thin layer of manganese oxides on an electronically conductive carbonaceous substrate with a high specific surface area is a promising approach to promoting the pseudocapacitance of manganese oxides in both organic and aqueous electrolytes.

The aim of this study is to improve the pseudocapacitive properties of manganese oxide in aqueous 1.0 M KCl and non-aqueous organic 1.0 M $LiClO_4$ in propylene carbonate (PC) electrolytes by preparing a thin film of manganese oxide on carbon nanotube film substrates with three-dimensional nanostructures. Among the various carbonaceous materials, CNTs are attractive substrate materials due to their chemical stability, good conductivity, and large surface area. CNTs have uniform diameters of several tens of nanometers, and unique properties such as entanglement with a nanoporous character. When CNTs are fabricated in the form of a thin film with a three-dimensional nanoporous structure, the CNT film is expected to provide an ideal substrate in terms of its electronic conductivity, specific surface area, and interconnected pore structure on the nanometer scale [15]. In this study, thin films of manganese oxides coated on three-dimensional nanoporous CNT film substrates are prepared by electrodeposition. The pseudocapacitive properties of the manganese oxides on the CNT film substrates are measured in 1.0 M KCl aqueous electrolyte in comparison with those in 1.0 M $LiClO_4$/PC organic electrolyte. Manganese oxide films are also electrodeposited on flat Pt-coated Si wafer substrates as reference samples for pseudocapacitive property comparison with the manganese oxides on CNT film substrates in both aqueous and organic electrolytes.

2. Experimental

2.1. Synthesis of manganese oxides electrodeposited on three-dimensional CNT film and flat Pt substrates

A CNT film substrate with a three-dimensional network structure was prepared on a Pt-coated Si wafer (Pt/Si wafer) by the electrostatic spray deposition technique. The detailed procedure used for the preparation of the CNT film substrate is described elsewhere [37]. The multiwalled CNTs (MWNTs), which were used in the preparation of the CNT film substrate, were supplied by ILJIN Nanotech Co., Ltd. The nominal area, thickness and mass of the CNT film were 1 cm × 1 cm, 7.0 ± 0.3 μm and 0.51 ± 0.02 mg cm^{-2}, respectively. In this study, the CNT film substrate contained no binders or conducting agents, thereby removing any uncertainties that might have arisen from their influences on the electrochemistry. The potential pulse electrodeposition technique was used to obtain a uniform oxide coating of MnO_2 on the three-dimensional nanoporous CNT film substrate through the entire film thickness. After the initial application of 1.0 V *vs.* saturated calomel electrode (SCE) in 0.2 M $MnSO_4{\cdot}5H_2O$ solution for 10 s, a potential pulse with an amplitude of 1.0 V *vs.* SCE and pulse-on time and pulse-off time of 0.3 and 2.1 s, respectively, was applied for 50 cycles using a multichannel potentiostat/galvanostat (VMP2, Princeton Applied Research, USA). The electrode was dried at 80 °C for 5 h after deposition. For comparison, manganese oxide on a Pt/Si wafer substrate was also prepared by potentiostatic electrodeposition at 1.0 V *vs.* SCE in the same 0.2 M $MnSO_4{\cdot}5H_2O$ deposition solution. Our previous X-ray absorption and Raman spectroscopy studies on the manganese oxides electrodeposited on carbon paper substrates in the same $MnSO_4{\cdot}5H_2O$ deposition solution showed that the deposited manganese oxide had a chemical formula of $MnO_2{\cdot}xH_2O$ with an amorphous structure [38]. Therefore, the electrodeposited manganese oxides on the CNT film and flat Pt/Si wafer substrates are hereafter denoted as the MnO_2/CNT and MnO_2 film electrodes, respectively. The amount of deposited manganese oxide was measured by weighing the difference between the CNT film or Pt/Si wafer substrates and the manganese oxide deposited-substrates after drying with a microbalance (Sartorius Ultra-Microbalance SC2). The readability and permissable tolerance of SC2 are 0.0001 and ±0.0007 mg, respectively. The amount of electrodeposited manganese oxides on the CNT film and Pt/Si wafer substrates was controlled to be ~0.10 mg.

2.2. Characterization

The morphologies of the MnO_2 film and MnO_2/CNT electrodes were observed by scanning electron microscopy (SEM, FEI-Company SIRION^{TM}). The nanostructure of the MnO_2/CNT electrode was examined using transmission electron microscopy (TEM, JEM-3000, JEOL). The characterization of the crystal structure of manganese oxide was based on XRD measurements (Rigaku DMAX-2500 diffractometer). No crystalline X-ray diffraction peaks were observed, except for the characteristic graphitic (0 0 2) peak of the MWNTs at $2\theta = 26°$, indicating the X-ray amorphous structure of the manganese oxides electrodeposited on the CNT film substrates. The manganese oxides electrodeposited on the Pt/Si wafer substrates also showed a similar amorphous structure. Electrochemical measurements in an aqueous electrolyte (1.0 M KCl) were conducted in a three-electrode beaker-type cell in which the manganese oxide electrodes were used as the working electrodes, a platinum plate was the counter electrode, and a saturated calomel electrode was the reference electrode. For electrochemical measurements in a non-aqueous electrolyte consisting of 1.0 M $LiClO_4$ in propylene carbonate ($LiClO_4$/PC), a three-electrode beaker-type cell was also used with different cell configurations. Lithium foils were used as the counter and reference electrodes.

All electrochemical measurements using the $LiClO_4$/PC electrolyte were carried out in an argon-filled glove box.

3. Results and discussion

3.1. Microstructures of MnO_2/CNT and MnO_2 film electrodes

Fig. 1 shows the microstructures of the bare CNT film substrate and manganese oxide coated on the CNT film substrate (i.e., MnO_2/CNT electrode). In Fig. 1(a), it is observed that the bare CNT film substrate is composed of nanotubes with diameters ranging from 15 to 40 nm entangled to form a uniform web with a three-dimensional nanoporous network structure. Compared with the bare CNT film substrate, the microstructure of the MnO_2/CNT electrode shown in Fig. 1(b) reveals that the diameter of the MnO_2-coated nanotubes is slightly increased, resulting in a decrease in the pore size. The diameter of the MnO_2-coated nanotubes ranges from 25 to 50 nm. This increase in the nanotube diameter in the MnO_2/CNT electrodes suggests that the coating of the manganese oxide on the individual CNTs occurred via electrochemical deposition. On the other hand, the cross-sectional SEM image of the MnO_2/CNT electrode (Fig. 1(c)) shows that the pore openings in the CNT film substrate are not blocked by MnO_2 deposits, thus allowing it to maintain its three-dimensional nanoporous network structure. The TEM image of the MnO_2/CNT film electrode depicted in Fig. 1(d) indicates that manganese oxide layers with thickness of approximately 3–5 nm are coated on the outer surface of the individual multiwalled carbon nanotubes. This result reveals that the manganese oxides nucleate heterogeneously *via* electrochemical deposition and are uniformly deposited on the individual CNTs at the nanometer scale. The three-dimensional nanoporous network structure of the MnO_2/CNT electrode is expected to provide an oxide|electrolyte interface with a large area, enhanced electronic conductivity and facile ion transport in the electrode, thereby improving the specific capacitance and high-rate capability of the manganese oxide.

The SEM images of the electrodeposited manganese oxide film on the flat Pt/Si wafer substrate (i.e., MnO_2 film electrode) are

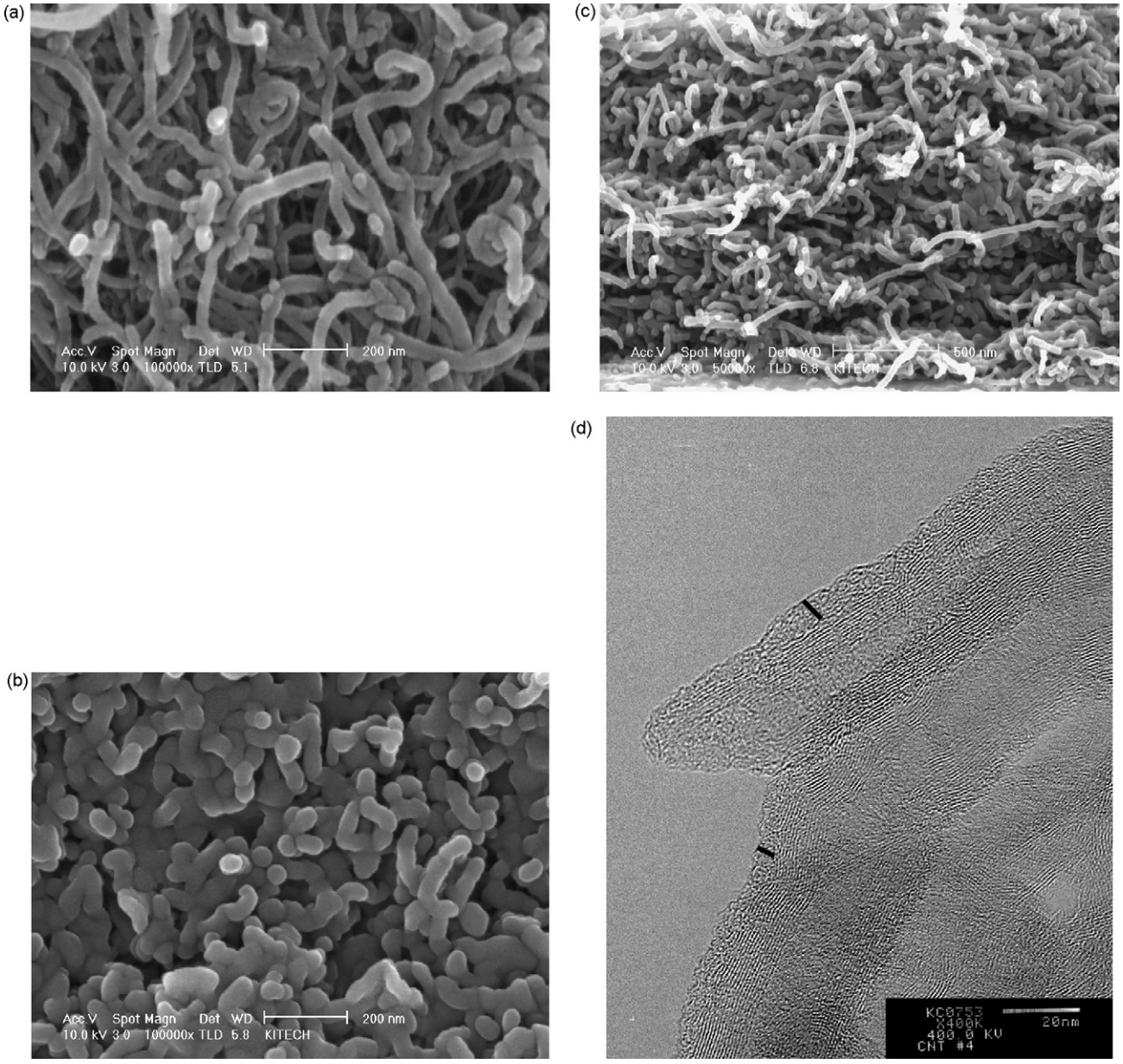

Fig. 1. SEM images of (a) bare CNT substrate; (b and c) MnO_2/CNT electrode; (d) TEM image of MnO_2/CNT electrode.

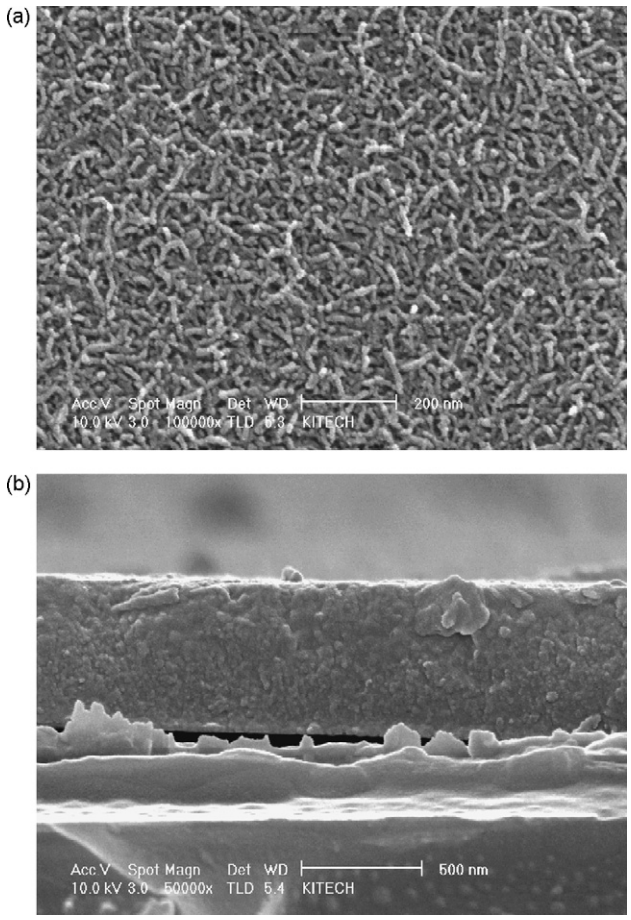

Fig. 2. SEM images of MnO_2 film electrode showing (a) top and (b) cross-sectional views.

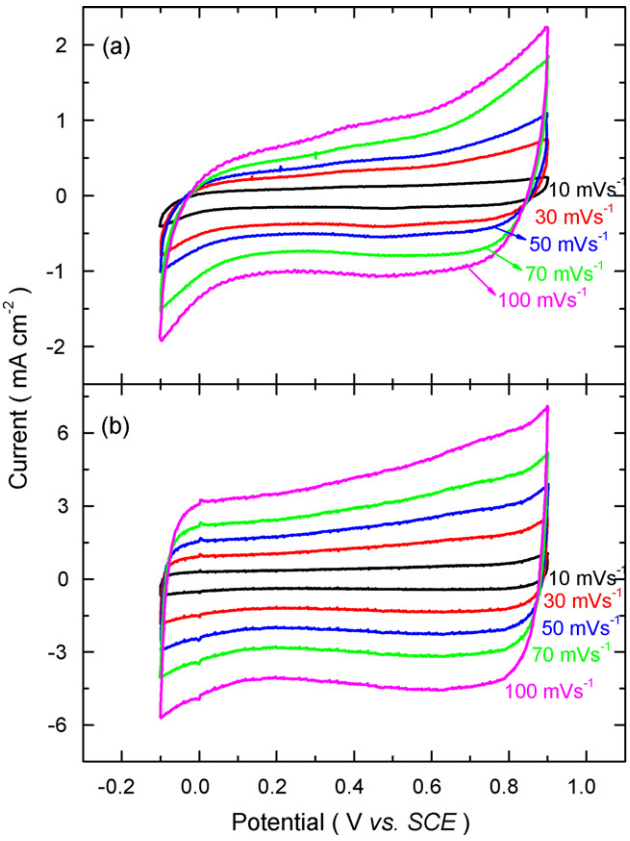

Fig. 3. CVs for (a) MnO_2 film and (b) MnO_2/CNT electrodes measured at scan rates from 10 to 100 mV s^{-1} in 1.0 M KCl aqueous electrolyte. Potential window: −0.1 to 0.9 V *vs.* SCE.

shown in Fig. 2(a) and (b), where the surface and cross-section of the MnO_2 film electrode are depicted, respectively. It can be seen that the manganese oxide electrodeposited on the Pt-coated Si wafer substrate is composed of short nanorods with a mean diameter of ca. 10 nm, as shown in Fig. 2(a). A similar microstructure was reported for manganese oxide film electrodes prepared by potentiostatic electrodeposition [18]. From the cross-sectional SEM image in Fig. 2(b), it can be seen that the nanorods are entangled with each other to form relatively compact layers with a thicknesses of ~0.64 μm.

3.2. *Electrochemical properties of MnO_2/CNT and MnO_2 film electrodes in 1.0 M KCl aqueous electrolyte*

Cyclic voltammetry was performed to investigate the electrochemical properties of the MnO_2 film and MnO_2/CNT electrodes in the aqueous electrolyte. Fig. 3(a) and (b) shows the cyclic voltammograms (CVs) of the MnO_2 film and MnO_2/CNT electrodes, respectively, which were measured at various scan rates ranging from 10 to 100 mV s^{-1} in the 1.0 M KCl aqueous electrolyte. The electrode potential was scanned between −0.1 and 0.9 V *vs.* SCE (i.e., a voltage window of 1.0 V). Although both electrodes exhibit capacitive behaviour with featureless current responses in their CVs, the MnO_2/CNT electrode shows the characteristic CV of an ideal capacitor compared with that of the MnO_2 film electrode. It is believed that the capacitive current responses of the MnO_2/CNT electrode in the CV curves are due to the redox reaction of the coated manganese oxide, since the whole CNT surface seems to be coated with manganese oxide, as confirmed by the SEM and TEM images in Fig. 1(b) and (d), respectively. Because the amounts of manganese oxide on both the Pt/Si wafer and CNT substrates are nearly the same, viz. ~0.10 mg cm^{-2}, the higher current response in the CVs of the MnO_2/CNT electrode implies that its specific capacitance is higher than that of the MnO_2 film electrode. In addition, extremely sharp current reversals at both ends of the potential limits are observed in the CV of the MnO_2/CNT electrode, even at a scan rate of 100 mV s^{-1}. On the other hand, the CV of the MnO_2 film electrode became slightly distorted and displays delayed current reversals at both ends of the potential limits with increasing scan rate. Therefore, it is clearly seen that the MnO_2/CNT electrode has far better electrochemical reversibility than the MnO_2 film electrode.

The specific capacitances were calculated from CVs at scan rates ranging from 10 to 100 mV s^{-1} to compare the rate capability of the MnO_2 film and MnO_2/CNT electrodes in aqueous solution. The specific capacitance values were determined by the following equation:

$$C_p = \frac{q_a + |q_c|}{2m\,\Delta V} \quad (2)$$

where C_p, q_a, q_c, m, and ΔV are the specific capacitance, the anodic and cathodic voltammetric charges on the positive and negative-going scans, the mass of the oxide deposit, and the potential range of the CV, respectively. Fig. 4(a) shows the specific capacitance with respect to the scan rate for the MnO_2 film and MnO_2/CNT electrodes in 1.0 M KCl electrolyte. The specific capacitances of the MnO_2 film and MnO_2/CNT electrodes based on the mass of oxide at 10 mV s^{-1} are 127 and 471 F g^{-1}, respectively. It has been reported that the pseudocapacitance of manganese oxide in aqueous neutral electrolytes could be attributed to the following redox reaction [17,38–40]:

$$MnO_2 + \delta C^+ + \delta e^- \leftrightarrow MnOOC_\delta \quad (3)$$

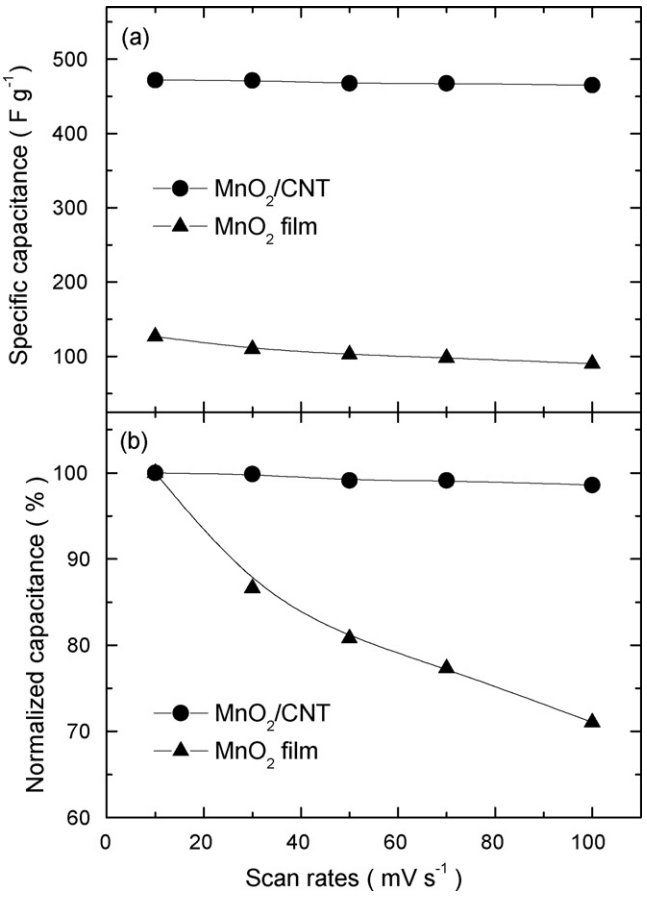

Fig. 4. (a) Specific and (b) normalized capacitances of MnO_2 film and MnO_2/CNT electrodes with respect to scan rates in 1.0 M KCl aqueous electrolyte.

where C^+ corresponds H^+ or alkali metal cations such as Na^+ and K^+. On the basis of Faraday's law, the theoretical specific capacitance of the stoichiometric reduction of Mn(IV)O_2 to Mn(III)OOC is approximately 1100 F g^{-1} with a voltage window of 1.0 V [24,38,41]. The active mass utilizations for the manganese oxides in the MnO_2 film and MnO_2/CNT electrodes at 10 mV s^{-1} in 1.0 M KCl are approximately 12 and 43%, respectively. This means that 12 and 43% of the manganese sites in the MnO_2 film and MnO_2/CNT electrodes could participate in the electrochemical reaction, respectively, within the potential range of −0.1 to +0.9 V *vs.* SCE in the 1.0 M KCl aqueous electrolyte. The MnO_2/CNT electrode shows ~4 times higher electrochemical utilization of the MnO_2 active material than the MnO_2 film electrode. It should be noted that the specific capacitance of the MnO_2/CNT electrodes remains unchanged, even when the scan rate is increased from 10 to 100 mV s^{-1}, whereas a moderate decrease in the capacitance of the MnO_2 film electrode is observed. To obtain a clear comparison of the rate capabilities of the two electrodes, the normalized capacitances obtained by dividing the specific capacitances of the electrodes at each scan rate by the specific capacitance measured at 10 mV s^{-1} are also plotted in Fig. 4(b). The decreases in the specific capacitance of the MnO_2 film and MnO_2/CNT electrodes from 10 to 100 mV s^{-1} is 29 and 2%, respectively, indicating the excellent rate capability of the MnO_2/CNT electrode. It is believed that the three-dimensional nanoporous structure of the MnO_2/CNT electrode can provide a much larger interfacial area between the oxide and electrolyte, improved electron conduction through the CNT web, and facile ionic transfer within the nanopores. Therefore, the improved specific capacitance and excellent rate capability of the MnO_2/CNT electrode compared with those of the MnO_2 film electrode are attributed to its three-dimensional nanoporous structure, which is obtained by coating manganese oxide with a thickness of 3–5 nm on the CNT film substrate. This result reveals that constructing an oxide electrode with a three-dimensional nanoporous structure offers a promising way to improve the specific capacitance and high-rate capability of aqueous electrolyte-based pseudocapacitors.

3.3. Electrochemical properties of MnO_2/CNT and MnO_2 film electrodes in 1.0 M $LiClO_4$/PC organic electrolyte

In order to examine the electrochemical properties of the MnO_2 film and MnO_2/CNT electrodes in an organic electrolyte, CVs at scan rates ranging from 10 to 100 mV s^{-1} were carried out in 1.0 M $LiClO_4$/PC. Fig. 5(a) and (b) shows the measured CVs of the MnO_2 film and MnO_2/CNT electrodes, respectively, within the potential window of 1.5–4.0 V *vs.* Li/Li$^+$ (i.e., a voltage window of 2.5 V). The insets in Fig. 5(a) and (b) are the CVs of the MnO_2 film and MnO_2/CNT electrodes, respectively, measured at 10 mV s^{-1}, showing their detailed shape at a slow scan rate. Interestingly, the CVs for the MnO_2 film and MnO_2/CNT electrodes in the 1.0 M $LiClO_4$/PC electrolyte exhibit substantially different features from those measured in the 1.0 M KCl electrolyte, as shown in Fig. 3(a) and (b). While the CVs of the MnO_2/CNT electrode clearly show featureless current responses representing pseudocapacitive behaviour, the CVs of the MnO_2 film electrode do not show typical capacitive characteristics. The CV of the MnO_2 film electrode at 10 mV s^{-1} (inset of Fig. 5(a)) is close to that of a battery electrode, even though it shows somewhat distorted capacitive current responses in the negative- and positive-going scans. A distinct current peak at 3.1 V followed by very small and broad current hump at around 3.5 V in the positive-going scan and two corresponding small and broad current peaks at around

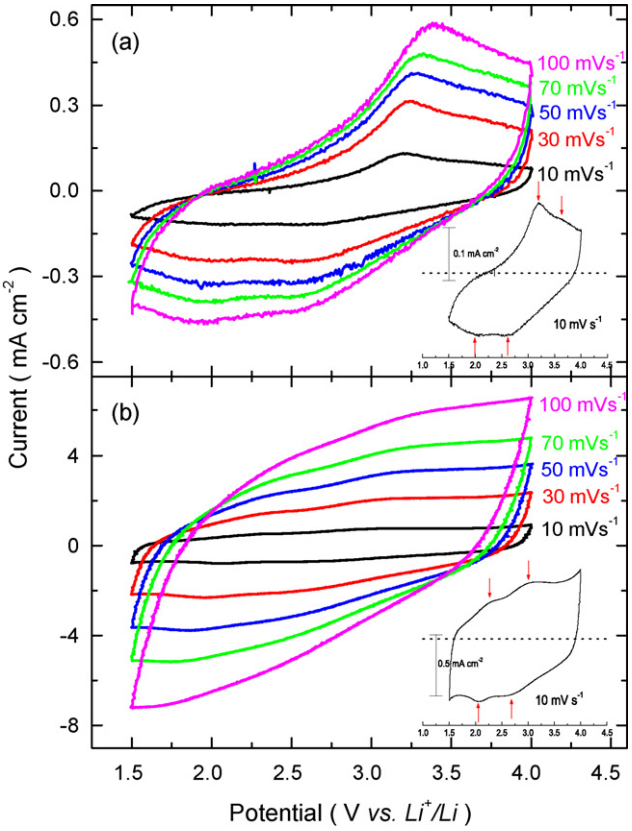

Fig. 5. CVs for (a) MnO_2 film and (b) MnO_2/CNT electrodes measured at scan rates ranging from 10 to 100 mV s^{-1} in 1.0 M $LiClO_4$/PC organic electrolyte. Potential window: 1.5–4.0 V *vs.* Li/Li$^+$. Insets: CVs at 10 mV s^{-1}. Arrows in insets indicate redox peaks.

2.6 and 2.0 V in the negative-going scan are seen in the CV of the MnO_2 film electrode at 10 mV s^{-1}. On the other hand, the CV of the MnO_2/CNT electrode at 10 mV s^{-1} (inset of Fig. 5(b)) exhibits two small and broad anodic current peaks at around 2.2 and 2.9 V and two corresponding cathodic peaks at around 2.6 and 2.0 V superimposed by large capacitive currents. It should be noted that the current responses of the MnO_2/CNT electrode in 1.0 M $LiClO_4$/PC are attributable to the redox reaction of the coated manganese oxide, because Li intercalation into bare CNTs has been reported to occur at potentials lower than 1.5 V *vs.* Li/Li^+ in $LiClO_4$/PC [42,43].

It has been reported that the redox reaction of manganese dioxide materials in lithium-containing organic electrolytes can be described by the following Li^+ intercalation/de-intercalation reaction [2,5,6]:

$$MnO_2 + \delta Li^+ + \delta e^- \leftrightarrow Li_\delta MnO_2 \quad (4)$$

where δ is the number of moles of Li ions and electrons participating in the reaction. The appearance of the two redox peaks in the CVs for both the MnO_2 film and MnO_2/CNT electrodes suggests that the Li^+ intercalation/de-intercalation reaction occurs via a two-step process. The very weak and broad features of the redox peaks for the MnO_2 film and MnO_2/CNT electrodes in Fig. 5(a) and (b), respectively, are attributed to the highly disordered structure of the electrodeposited amorphous manganese oxide in the MnO_2 film and MnO_2/CNT electrodes [2,4]. The differences in the redox peak potentials of the MnO_2 film are 1.1 and 0.9 V, whereas those of the MnO_2/CNT electrodes are 0.2 and 0.3 V for the first and second redox peaks, respectively. The MnO_2/CNT electrode shows much smaller differences in peak potential than the MnO_2 film electrode, which indicates more facile and reversible Li^+ intercalation/de-intercalation in the former case. When the scan rate is increased from 10 to 100 mV s^{-1}, the CVs of the MnO_2/CNT electrode maintain their capacitive characteristics which demonstrates the good high-rate capability of the MnO_2/CNT electrode even in the organic electrolyte.

For V_2O_5 materials, Rolison and Dunn [44] reported that the origin of the capacitive behaviour of very thin layers of V_2O_5 might be associated with the high surface area of the aerogel materials [44]. Recently, Okubo et al. [36] reported the existence of a nanosize effect on the discharge characteristics of $LiCoO_2$ cathode material for Li-ion batteries and showed that the capacitive behaviour became stronger as the crystallite size decreased on the nanometer scale (i.e., 17–6 nm). The discharge curve for the intercalation of Li^+ in bulk $LiCoO_2$ crystals (i.e., constant voltage upon discharge) became capacitive (i.e., linear decline of voltage upon discharge) when the number of surface layers was increased by decreasing the crystallite size. Therefore, the difference in electrochemical activity between the MnO_2 film and MnO_2/CNT electrodes in the 1.0 M $LiClO_4$/PC electrolyte may be due to the significantly increased oxide/electrolyte interfacial area in the MnO_2/CNT electrode.

The specific capacitances of the MnO_2/CNT electrode in 1.0 M $LiClO_4$/PC at scan rates from 10 to 100 mV s^{-1} were calculated using Eq. (2) to examine the rate capability of the electrode. Even though the MnO_2 film electrode does not show capacitive behaviour in 1.0 M $LiClO_4$/PC, the specific capacitances were calculated for comparison purposes. The specific capacitances of the MnO_2 film and MnO_2/CNT electrodes in 1.0 M $LiClO_4$/PC on the basis of the mass of oxide at 10 mV s^{-1} are 72 and 576 F g^{-1}, respectively, see Fig. 6(a). When 1 mol of Li ions and electrons participate in the reaction, the Mn^{4+} in MnO_2 is reduced to Mn^{3+}, and the theoretical specific capacitance of MnO_2 calculated on the basis of reaction (4) corresponds to 440 F g^{-1} with a voltage window of 2.5 V. Considering the theoretical specific capacitance, 1.3 mol of Li^+ participate in the redox reaction of the MnO_2/CNT electrode at 10 mV s^{-1} in 1.0 M $LiClO_4$/PC. It has been reported [3,4] that the intercalation

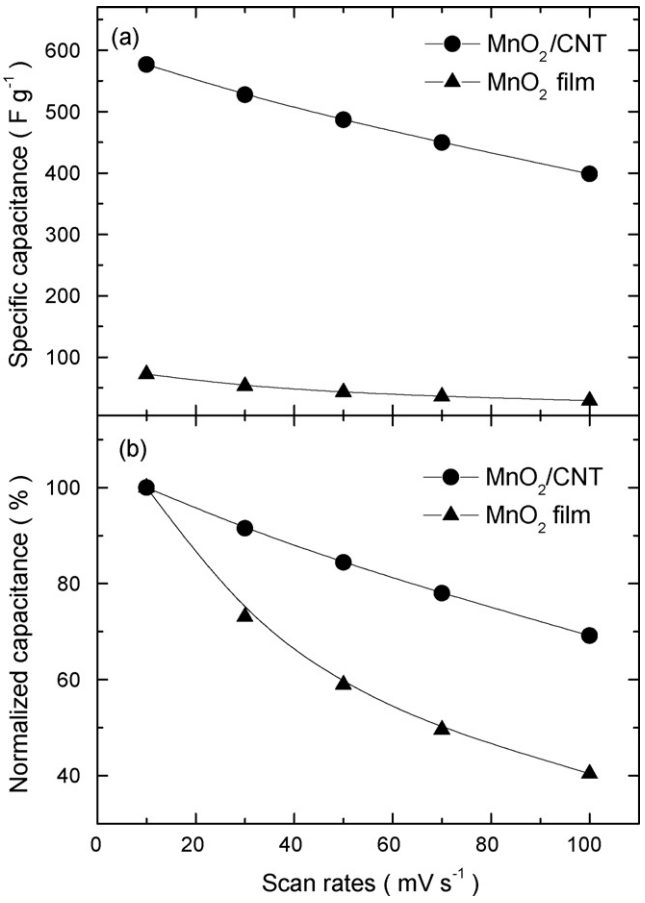

Fig. 6. (a) Specific and (b) normalized capacitances of MnO_2 film and MnO_2/CNT electrodes with respect to scan rates in 1.0 M $LiClO_4$/PC organic electrolyte.

capacity of amorphous manganese oxide-based cathode materials in lithium ion batteries involve the Mn^{3+}/Mn^{2+} couple in addition to the Mn^{4+}/Mn^{3+} couple and exhibit an insertion/extraction of more than 1.0 mol of Li^+. Hibino et al. [33] reported that the change in the valence state of manganese from Mn^{4+} to Mn^{3+} and from Mn^{3+} to Mn^{2+} was responsible for the two regions above and below ~2.0 V *vs.* Li/Li^+ in the discharge curve of composite materials of sodium manganese oxide and acetylene black in $LiClO_4$ dissolved in ethylene carbonate:dimethoxyethane (1:1) [33]. Therefore, the participation of 1.3 mol of Li^+ in the redox reaction of the MnO_2/CNT electrode may be explained by a change in the valence state of manganese from Mn^{4+} to Mn^{3+} as well as that from Mn^{3+} to Mn^{2+}. On the other hand, only 0.16 mol of Li^+ participate in the redox reaction in the case of the MnO_2 film electrode. Because an electrochemical reaction would be initiated from the surface layer of the manganese oxides in contact with the electrolyte, and Li^+ diffusion within manganese oxide is involved, a large proportion of the oxide inside the MnO_2 film electrode may act as a dead volume and not participate in the electrochemical reaction, resulting in the low electrochemical utilization of the MnO_2 film electrode. Furthermore, the low electrical conductivity could result in the low electrochemical utilization of the MnO_2 film electrode, since there are no conducting additives within it. The detailed redox reaction mechanism of the MnO_2 film and MnO_2/CNT electrodes in an organic electrolyte is currently under investigation using X-ray absorption spectroscopy.

Fig. 6(b) shows the normalized capacitances of the MnO_2 film and MnO_2/CNT electrodes with respect to scan rate in the range from 10 to 100 mV s^{-1}. The decreases in the specific capacitance of the MnO_2 film and MnO_2/CNT electrodes as the potential scan rate is increased from 10 to 100 mV s^{-1} is 60 and 31%, respectively. This

demonstrates the far better high-rate capability of the MnO_2/CNT electrode. It is believed that the high specific capacitance and good rate capability of the MnO_2/CNT electrode in $LiClO_4$/PC are due to the construction of a three-dimensional nanoporous structure consisting of the thin manganese oxide layer on the CNT film substrate at the nm scale. This results in shortening of the Li^+ diffusion distance, improved electron conduction through the CNT web, and facile Li^+ ion transfer to the reaction sites.

3.4. Comparison of pseudocapacitance of MnO_2/CNT electrode in aqueous and organic electrolytes

We considered that it would be interesting to compare the specific capacitance and rate capability of the MnO_2/CNT electrode in the 1.0 M KCl and 1.0 M $LiClO_4$/PC electrolytes. The specific charge (i.e., specific capacitance multiplied by voltage) of the MnO_2/CNT electrode in the 1.0 M KCl and 1.0 M $LiClO_4$/PC electrolytes at 10 mV s^{-1} is 471 and 1440 C g^{-1}, respectively. Considering the theoretical capacity of 1100 C g^{-1} for MnO_2, it can be concluded that 1.3 mol of Li^+ participated in the redox reaction in 1.0 M $LiClO_4$/PC, whereas only 0.43 mol of H^+ or K^+ could participate in the redox reaction in 1.0 M KCl. These findings reveal that the redox reaction of the MnO_2/CNT electrode in 1.0 M KCl should be confined to the outer part of the manganese oxide layers at a maximum depth of ~2 nm, while the redox reaction in 1.0 M $LiClO_4$/PC involves Li^+ diffusion into the whole 3–5 nm thick manganese oxide layers. This hypothesis is also supported by the better high-rate capability of the MnO_2/CNT electrode in 1.0 M KCl than in 1.0 M $LiClO_4$/PC, with a decrease in the capacitance of 2% being observed in 1.0 M KCl compared with 31% in 1.0 M $LiClO_4$/PC when the scan rate is increased from 10 to 100 mV s^{-1}. Because the MnO_2/CNT electrode shows typical capacitive behaviour with a high specific capacitance in both the aqueous and organic electrolytes, it has the potential to be used as an electrode in both aqueous electrolyte-based supercapacitors, where the power is more critical than the energy, and in organic electrolyte-based supercapacitors, where the energy is more critical than the power. Compared with the MnO_2 film electrode, the MnO_2/CNT electrode shows a much higher specific capacitance and better high-rate capability, regardless of the electrolyte used. This emphasizes that an oxide|electrolyte interface with a large interfacial area, facile electrolyte transportation and a good electronic conduction path through the entire electrode are essential to ensure the improved specific capacitance and high-rate capability of supercapacitor electrodes.

Fig. 7 gives the discharge curves of the MnO_2/CNT electrode in the 1.0 M KCl and 1.0 M $LiClO_4$/PC electrolytes measured at three discharge currents of 5, 10 and 20 A g^{-1} based on the mass of the manganese oxide. The MnO_2/CNT electrode in 1.0 M $LiClO_4$/PC was discharged from 4.0 to 1.5 V *vs.* Li/Li^+, while the MnO_2/CNT electrode in 1.0 M KCl was discharged from +0.9 to −0.1 V *vs.* SCE. The discharge curves of the MnO_2/CNT electrodes in 1.0 M $LiClO_4$/PC and 1.0 M KCl clearly show a linear decline of potential at the given operating voltages of 2.5 and 1.0 V, respectively, which is characteristic of capacitive behaviour. The MnO_2/CNT electrode has better high-rate capability in the 1.0 M KCl than in the 1.0 M $LiClO_4$/PC electrolyte. The discharge specific capacitance of the MnO_2/CNT electrode in the 1.0 M KCl electrolyte at discharge currents of 5, 10 and 20 A g^{-1} is 463, 448, and 423 F g^{-1}, while the corresponding values in the 1.0 M $LiClO_4$/PC electrolyte are 491, 455 and 402 F g^{-1}, respectively.

Fig. 8 shows the cycling stability of the MnO_2/CNT electrode measured by constant-current charging/discharging at 10 A g^{-1} for 100 cycles in the 1.0 M KCl aqueous and 1.0 M $LiClO_4$/PC organic electrolytes. The MnO_2/CNT electrode cycled in 1.0 M KCl has much better cycling stability than that cycled in 1.0 M $LiClO_4$/PC, showing ~9% decrease in the initial capacitance after 100 cycles. On the other hand, there is a ~34% decrease in the initial capacitance

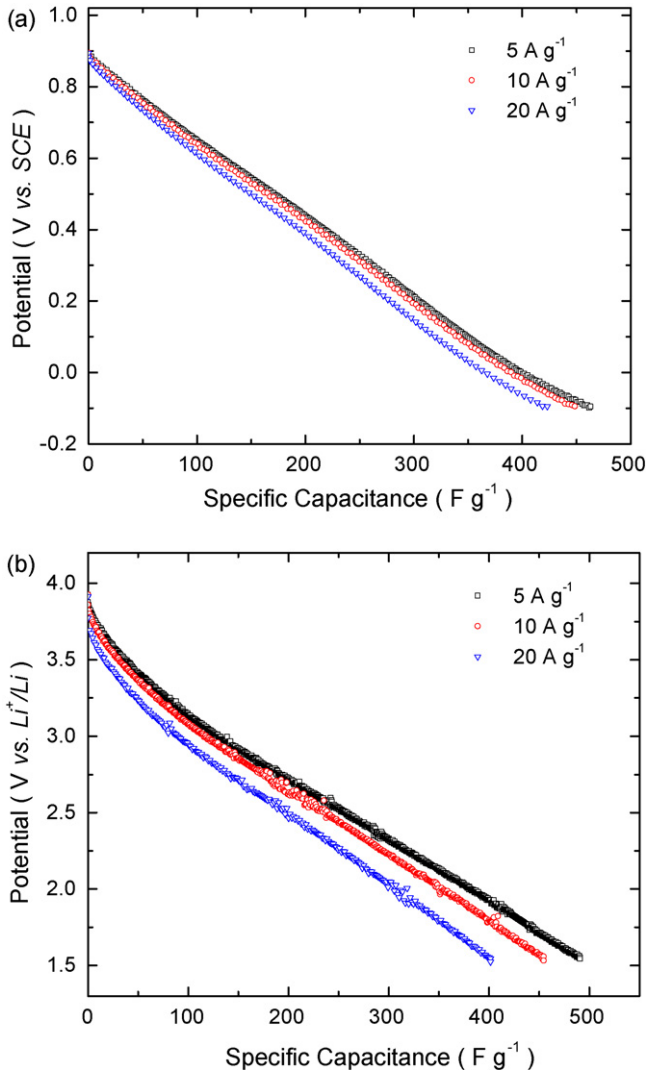

Fig. 7. Discharge curves of MnO_2/CNT electrode with discharge current densities in (a) 1.0 M KCl aqueous and (b) 1.0 M $LiClO_4$/PC organic electrolytes.

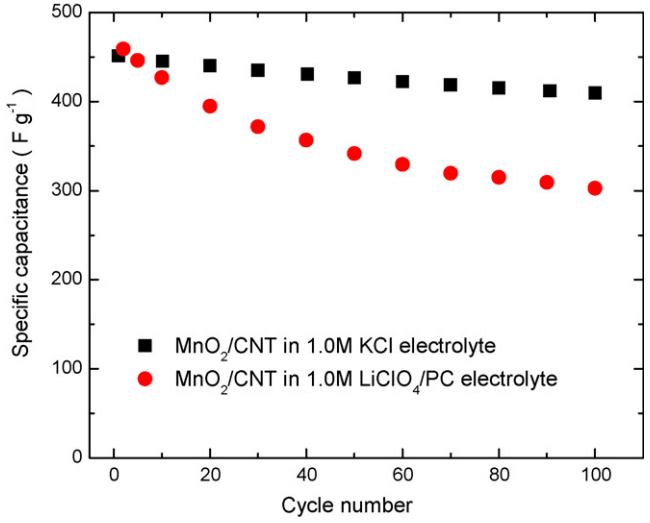

Fig. 8. Cycelability of MnO_2/CNT electrodes measured by constant-current charging/discharging at 10 A g^{-1} in 1.0 M KCl aqueous and 1.0 M $LiClO_4$/PC organic electrolytes.

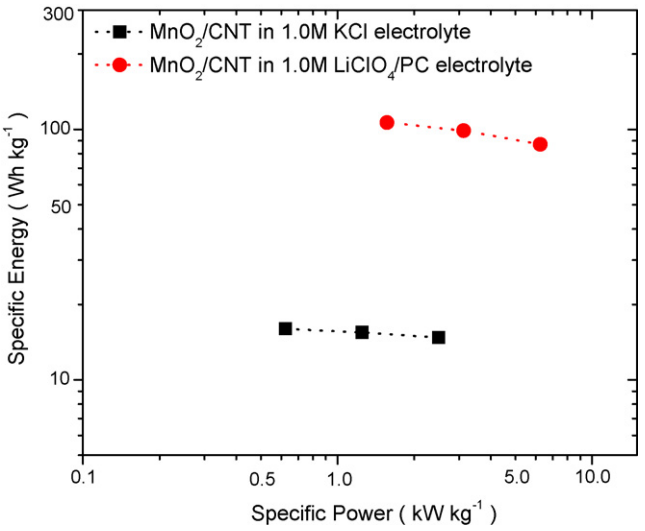

Fig. 9. Ragone plots for capacitors composed of two identical MnO_2/CNT electrodes using 1.0 M KCl aqueous and 1.0 M $LiClO_4$/PC organic electrolytes. Weight of manganese oxide active materials is considered for calculation of specific energy and power.

for the MnO_2/CNT electrode in 1.0 M $LiClO_4$/PC after 100 cycles. Lattice distortion due to the Jahn–Teller effect occurs when the average oxidation state of the manganese ions is below 3.5, because manganese ions in the trivalent and high spin state are associated with Jahn–Teller distortion [2]. Based on the specific capacitance and electrochemical utilization of the MnO_2/CNT electrode measured in 1.0 M KCl and 1.0 M $LiClO_4$/PC, discharge of the MnO_2/CNT electrode to 1.5 V *vs.* Li/Li^+ in 1.0 M $LiClO_4$/PC could result in reduction of the average oxidation state of the manganese ions below 3.0, whereas only 0.43 mol of Mn^{4+} are reduced to Mn^{3+} in 1.0 M KCl. Therefore, structural distortion of the manganese oxide in the MnO_2/CNT electrode upon discharge in 1.0 M $LiClO_4$/PC could cause it to exhibit relatively poor cycleability compared with that in 1.0 M KCl. Nonetheless, further studies are needed to understand the origin of the capacitance fading and improve the cycleability of the MnO_2/CNT electrode in the 1.0 M $LiClO_4$/PC organic electrolyte. Attempts such as the optimization of the heat treatment and structure stabilization by the doping of non-electrochemically active elements are possible ways to enhance the cycleability of the MnO_2/CNT electrode in organic electrolytes.

3.5. Ragone plot of MnO_2/CNT electrode in aqueous and organic electrolytes

For a symmetric electrochemical capacitor composed of two identical MnO_2/CNT electrodes, the specific capacitance would be one-fourth of that of a single electrode in a half-cell. Taking into account the specific capacitance of the capacitor during discharge and the operating voltage of 1.0 and 2.5 V for the MnO_2/CNT electrode in the 1.0 M KCl and 1.0 M $LiClO_4$/PC electrolytes, respectively, the specific energy and power of the symmetric electrochemical capacitor are plotted in Fig. 9. It should be noted that these Ragone plots are only intended to serve as a comparison of the specific energy and power for symmetric electrochemical capacitors using aqueous and organic electrolytes on the basis of MnO_2/CNT electrodes, because the calculation does not include the packaging and all the cell components. For a specific power of 0.6 kW kg^{-1}, the specific energy of the capacitor using the 1.0 M KCl electrolyte is calculated to be 16.1 Wh kg^{-1}. When the specific power is increased to 2.5 kW kg^{-1}, a slight decrease in the specific energy to ~14.8 Wh kg^{-1} is observed for the capacitor with the 1.0 M KCl electrolyte. On the other hand, compared with the capacitor using the 1.0 M KCl electrolyte, the specific energy of the capacitor using the 1.0 M $LiClO_4$/PC electrolyte showed a significantly improved specific energy of 106.5 Wh kg^{-1} with a specific power of 1.6 kW kg^{-1}. The specific energy of the capacitor with 1.0 M $LiClO_4$/PC decreases to 87.3 Wh kg^{-1} when the specific power is increased to 6.3 kW kg^{-1}. Since the MnO_2/CNT electrode shows a similar specific capacitance of ~450 F g^{-1} in both 1.0 M KCl aqueous solution and $LiClO_4$/PC organic solution, the approximately six times enhancement of the specific energy for the capacitor using the organic electrolyte is due mainly to the increase in the potential window from 1.0 to 2.5 V. The significant improvement in the specific energy in the 1.0 M $LiClO_4$/PC electrolyte with a comparable power to that in the 1.0 M KCl electrolyte indicates that the construction of a three-dimensional nanoporous network structure consisting of a thin oxide layer on a CNT film substrate at the nm scale and the use of an Li-containing organic electrolyte could be an effective way to improve the specific energy of supercapacitors.

4. Conclusions

Thin amorphous manganese oxide layers with a thickness of 3–5 nm have been electrochemically deposited on a carbon nanotube film substrate having a three-dimensional nanoporous structure. From a comparative study of MnO_2 film and MnO_2/CNT electrodes in 1.0 M KCl aqueous and 1.0 M $LiClO_4$/PC organic electrolytes, only the MnO_2/CNT electrode shows pseudocapacitive behaviour in the organic electrolyte, while both electrodes display pseudocapacitive behaviour in the aqueous electrolyte. The difference in the electrochemical behaviour of the MnO_2 film and MnO_2/CNT electrodes in the organic electrolyte is associated with the significantly increased surface area and improved electron conduction path of the manganese oxide in the MnO_2/CNT electrode. Compared with the MnO_2 film electrode, the MnO_2/CNT electrode has a much higher specific capacitance and rate capability in both the aqueous and organic electrolytes. This is due to the construction of a three-dimensional nanoporous structure that consists of a thin manganese oxide layer on the CNT film substrate at the nm scale. This result emphasizes that an oxide|electrolyte interface with a large interfacial area, facile electrolyte transportation and good electronic conduction path through the entire electrode are essential to improve the specific capacitance and high-rate capability of supercapacitor electrodes.

For a symmetric electrochemical capacitor composed of two identical MnO_2/CNT electrodes, the device using the organic electrolyte is expected to show ~6 times higher specific energy (based on manganese oxide) than that using the aqueous electrolyte with little loss of specific power, due to the increase in the potential window from 1.0 to 2.5 V. This result reveals that the construction of a three-dimensional nanoporous network structure consisting of a thin oxide layer on a CNT film substrate at the nm scale and the use of a Li-containing organic electrolyte are prospective approaches to improving the specific energy of supercapacitors.

Acknowledgements

This work was supported by the Korea Science & Engineering Foundation (KOSEF) through the National Research Lab. Program funded by the Ministry of Science and Technology (No. R0A-2007-000-10042-0). The work at Brookhaven National Laboratory was supported by the Assistant Secretary for Energy Efficiency and Renewable Energy, Office of Vehicle Technologies, under the program of "Hybrid and Electric Systems", of the U.S. Department of Energy under Contract Number DEAC02-98CH10886.

References

[1] Y. Chabre, J. Pannetier, Prog. Solid State Chem. 23 (1995) 1–130.

[2] M.M. Thackeray, Prog. Solid State Chem. 25 (1997) 1–71.
[3] J.K. Kim, A. Manthiram, Nature 390 (1997) 265–267.
[4] J.J. Xu, J. Yang, Electrochem. Commun. 5 (2003) 230–235.
[5] F. Jiao, P.G. Bruce, Adv. Mater. 19 (2007) 657–660.
[6] J.Y. Luo, J.J. Zhang, Y.Y. Xia, Chem. Mater. 18 (2006) 5618–5623.
[7] M.H. Rossouw, D.C. Liles, M.M. Thackeray, Mater. Res. Bull. 27 (1992) 221–230.
[8] Y.H. Lee, J.B. Goodenough, J. Solid State Chem. 144 (1999) 220–223.
[9] S.C. Pang, M.A. Anderson, T.W. Chapman, J. Electrochem. Soc. 147 (2000) 444–450.
[10] J.P. Zheng, P.J. Cygan, T.R. Zow, J. Electrochem. Soc. 142 (1995) L6–L8.
[11] K.C. Liu, M.A. Anderson, J. Electrochem. Soc. 143 (1996) 124–130.
[12] K.W. Nam, K.B. Kim, J. Electrochem. Soc. 149 (2002) A346–A354.
[13] C. Lin, J.A. Ritter, B.N. Popov, J. Electrochem. Soc. 145 (1998) 4097–4103.
[14] Y.H. Lee, J.B. Goodenough, J. Solid State Chem. 148 (1999) 81–84.
[15] I.H. Kim, J.H. Kim, B.Y. Cho, Y.H. Lee, K.B. Kim, J. Electrochem. Soc. 153 (2006) A1451–A1458.
[16] R.N. Reddy, R.G. Reddy, J. Power Sources 124 (2003) 330–337.
[17] M. Toupin, T. Brousse, D. Belanger, Chem. Mater. 14 (2002) 3946–3952.
[18] C.C. Hu, T.W. Tsou, Electrochem. Commun. 4 (2002) 105–109.
[19] C.C. Hu, C.C. Wang, J. Electrochem. Soc. 150 (2003) A1079–A1084.
[20] J. Jiang, A. Kucernak, Electrochim. Acta 47 (2002) 2381–2386.
[21] V. Subramanian, H. Zhu, R. Vajtai, P.M. Ajayan, B. Wei, J. Phys. Chem. B 109 (2005) 20207–20214.
[22] K.W. Nam, K.B. Kim, J. Electrochem. Soc. 153 (2006) A81–A88.
[23] A. Zolfaghari, F. Ataherian, M. Ghaemi, A. Gholami, Electrochim. Acta 52 (2007) 2806–2814.
[24] S.B. Ma, K.W. Nam, W.S. Yoon, X.Q. Yang, K.Y. Ahn, K.H. Oh, K.B. Kim, J. Power Sources 178 (2008) 483–489.
[25] E. Raymundo-Pinero, V. Khomenko, E. Frackowiak, F. Beguin, J. Electrochem. Soc. 152 (2005) A229–A235.
[26] C.Y. Lee, H.M. Tsai, H.J. Chuang, S.Y. Li, P. Lin, T.Y. Tseng, J. Electrochem. Soc. 152 (2005) A716–A720.
[27] X. Xie, L. Gao, Carbon 45 (2007) 2365–2373.
[28] A.E. Fischer, K.A. Pettigrew, D.R. Rollison, R.M. Stroud, J.W. Long, Nano Lett. 7 (2007) 281–286.
[29] C. Wan, K. Azumi, H. Konno, Electrochim. Acta 52 (2007) 3061–3066.
[30] S. Zhu, H. Zhou, M. Hibino, I. Honma, M. Ichihara, Adv. Funct. Mater. 15 (2005) 381–386.
[31] X. Dong, W. Shen, J. Gu, L. Xiong, Y. Zhu, H. Li, J. Shi, J. Phys. Chem. B 110 (2006) 6015–6019.
[32] M. Hibino, H. Kawaoka, H. Zhou, I. Honma, J. Power Sources 124 (2003) 143–147.
[33] M. Hibino, H. Kawaoka, H. Zhou, I. Honma, Electrochim. Acta 49 (2004) 5209–5216.
[34] X. Huang, J. Yue, A. Attia, Y. Yang, J. Electrochem. Soc. 154 (2007) A26–A33.
[35] B.E. Conway, J. Electrochem. Soc. 138 (1999) 1539–1548.
[36] M. Okubo, E. Hosono, J. Kim, M. Enomoto, N. Kojima, T. Kudo, H. Zhou, I. Honma, J. Am. Chem. Soc. 129 (2007) 7444–7452.
[37] J.H. Kim, K.W. Nam, S.B. Ma, K.B. Kim, Carbon 44 (2006) 1963–1968.
[38] K.W. Nam, M.G. Kim, K.B. Kim, J. Phys. Chem. C 111 (2007) 749–758.
[39] V. Khomenko, E. Raymundo-Pinero, F. Beguin, J. Power Sources 153 (2006) 183–190.
[40] L. Athouel, F. Moser, R. Dugas, O. Crosnier, D. Belanger, T. Brousse, J. Phys. Chem. C 112 (2008) 7270–7277.
[41] S.L. Kuo, N.L. Wu, J. Electrochem. Soc. 153 (2006) A1317–A1324.
[42] E. Frackowiak, S. Gautier, H. Gaucher, S. Bonnamy, F. Beguin, Carbon 37 (1999) 61–69.
[43] G.T. Wu, C.S. Wang, X.B. Zhang, H.S. Yang, Z.F. Qi, P.M. He, W.Z. Li, J. Electrochem. Soc. 146 (1999) 1691–1701.
[44] D.R. Rolison, B. Dunn, J. Mater. Chem. 11 (2001) 963–980.